European Journal of Physics

PAPER

Using Biot–Savart's law to determine the finite tube's magnetic field

To cite this article: J M Ferreira and Joaquim Anacleto 2018 *Eur. J. Phys.* **39** 055202

IOP Publishing European Journal of Physics
Eur. J. Phys. **39** (2018) 055202 (14pp) https://doi.org/10.1088/1361-6404/aace84

Using Biot–Savart's law to determine the finite tube's magnetic field

J M Ferreira[1,2,4] **and Joaquim Anacleto**[1,3]

[1] Departamento de Física, Escola de Ciências e Tecnologia, Universidade de Trás-os-Montes e Alto Douro, Quinta de Prados, 5001-801 Vila Real, Portugal
[2] Laboratório de Instrumentação, Engenharia Biomédica e Física da Radiação (LIBPhys-UNL), Universidade Nova de Lisboa, 2829-516 Monte da Caparica, Portugal
[3] IFIMUP-IN and Departamento de Física e Astronomia, Faculdade de Ciências, Universidade do Porto, R. do Campo Alegre s/n, 4169-007 Porto, Portugal

E-mail: jferreir@utad.pt and anacleto@utad.pt

Received 9 April 2018, revised 4 June 2018
Accepted for publication 22 June 2018
Published 12 July 2018

Abstract

Biot–Savart's law is used to determine in all regions of space the magnetic field generated by a finite length conducting tube of negligible thickness. Simplified approximate closed form solutions for the magnetic field in the tube axis vicinity, near the median plane just outside the tube, and very far from the tube, are also derived. Lastly, the finite tubular conductor results are used to address the finite solenoid magnetic field's azimuthal component.

Keywords: Biot–Savart, tubular conductor, solenoid, magnetic field

1. Introduction

Biot–Savart's law is a fundamental and easy-to-use relation whose relevance derives, in part, from its potential as a tool to determine the magnetic field generated by the flow of current through different geometrical configurations, of which the most extensively addressed is probably the filamentary wire segment, e.g. [1–11] and references therein. By contrast, even though a finite length tubular conductor's magnetic field can be obtained by superposition of filamentary wire segments carrying infinitesimal current, Biot–Savart's law has not previously been applied to such problem, which as far as known to us has only been addressed in two recent studies [12, 13], of which [12] is the most relevant in the present context. In [12] the magnetic field of a finite length tubular conductor of negligible thickness was determined by

[4] Author to whom any correspondence should be addressed.

applying an oblique solid angle formula derived therein to an expression for magnetic field circulation obtained in [14] from the application of Ampère–Maxwell's law for magnetic field circulation to an arbitrarily-shaped finite length wire segment in the zero retarded-time limit. The present study aims to apply a different method, i.e. Biot–Savart's law, to obtain the finite tubular conductor magnetic field. Using distinct methods to solve the same problem, besides being instructive, allows the reader to evaluate the relative advantages and disadvantages of each. Moreover, though more elegant, the method used in [12] (including the oblique solid angle formula) is new and thus far from being widely adopted, the use of an alternative method contributing to corroborate the results in [12]. For instance, one could imagine calculating the vector potential and taking the curl to solve this problem. However, Biot–Savart's law already explicitly contains the magnetic field and thus provides a direct method of calculation. For this reason it is, together with Ampère's law, the most widely used for problem solving at the undergraduate level, e.g. [5, 15]. Most undergraduates will therefore be already familiar with its use to solve elementary problems such as the finite wire, and since the finite wire is the basic building block of a finite tube the adoption of Biot–Savart's law seems the natural choice to solve such problem. Being a study intended for undergraduates, we aim to use Biot–Savart's law to explore the symmetries that result from its application to the finite tubular conductor problem, leading to a description of its magnetic field from a physical perspective. Additionally, this study aims to (i) corroborate the results in [12]; (ii) obtain simplified expressions that approximate the magnetic field in the tube axis vicinity, near the median plane just outside the tube, and very far from the tube; (iii) use the finite length tubular conductor results to address the weak azimuthal component of the finite length solenoid field, thereby completing an analysis which has up to now been restricted to the exterior of an infinitely long solenoid, see [16–25].

2. Results and discussion

2.1. General solution for the finite tube's magnetic field

Consider an axial current I uniformly distributed around a thin tubular conductor (figure 1), of radius R and length L. Such tubular conductor can be divided into segments, each traversed by an elementary current $\mathrm{d}I$, the flow of $\mathrm{d}I$ through any infinitesimal length vector $\mathrm{d}\overrightarrow{l_1}$ originating an infinitesimal magnetic field $\mathrm{d}^2\overrightarrow{B_1}$ at point P, given by Biot–Savart's law as

$$\mathrm{d}^2\overrightarrow{B_1} = \frac{\mu_0}{4\pi}\mathrm{d}I\frac{\mathrm{d}\overrightarrow{l_1}\times\overrightarrow{s_1}}{s_1^3} = \frac{\mu_0}{4\pi}\mathrm{d}I\frac{\mathrm{d}\overrightarrow{l_1}\times\overrightarrow{r_1}}{s_1^3}, \tag{1}$$

where μ_0 is the permeability in free space, position vectors $\overrightarrow{s_1}$ and $\overrightarrow{r_1}$ are defined in figure 1, and the second equality in (1) follows directly from the vector product property $\mathrm{d}\overrightarrow{l_1}\times\overrightarrow{s_1} = \mathrm{d}\overrightarrow{l_1}\times\overrightarrow{r_1}$. Note that (1) is only valid as long as the current changes little in the time it takes a light signal to travel from the elementary segments to the point of interest, e.g. [8, 26], this being an assumption of the present study. To avoid unnecessary duplication only the case $0 \leqslant z_C \leqslant L/2$ is considered below, z_C being the z-coordinate of point P in figure 1. The extension to $z_C > L/2$, which involves minor changes to the equations, is addressed later, and the case $z_C < 0$ is redundant due to the symmetry of the problem.

The integration of (1) is trivial, giving the familiar expression for the magnitude of the magnetic field generated at P by a segment of wire traversed by a current $\mathrm{d}I$, i.e.

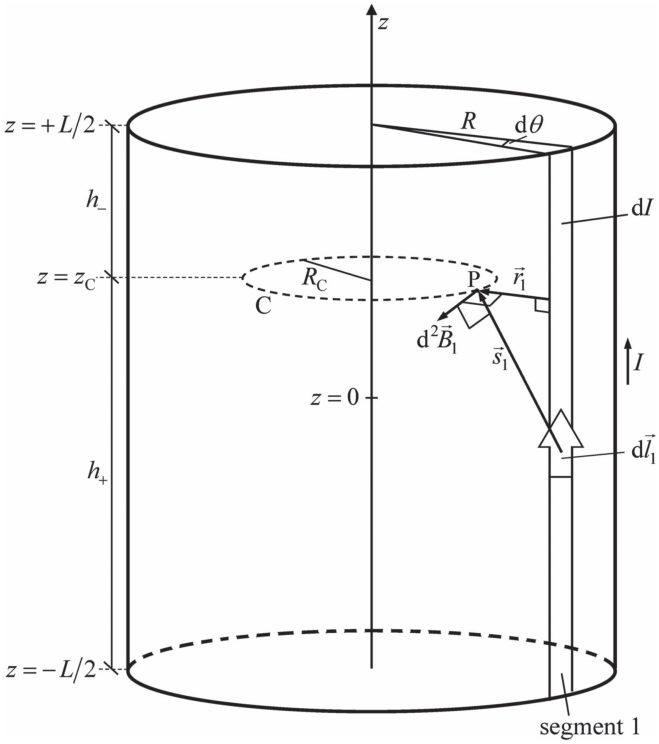

Figure 1. Tubular conductor (radius R) traversed by current I can be divided into segments (length L, width $R\,\mathrm{d}\theta$), each traversed by an elementary current $\mathrm{d}I$ whose direction determines that of infinitesimal length vector $\mathrm{d}\overrightarrow{l_1}$. The flow of $\mathrm{d}I$ through any $\mathrm{d}\overrightarrow{l_1}$ in segment 1 generates an infinitesimal field $\mathrm{d}^2\overrightarrow{B_1}$ at point P distant R_C from the z-axis. Position vectors of P relative to $\mathrm{d}\overrightarrow{l_1}$ and to the segment's closest point are, respectively, $\overrightarrow{s_1}$ and $\overrightarrow{r_1}$. From Biot–Savart's law $\mathrm{d}^2\overrightarrow{B_1}$ is always normal to both $\mathrm{d}\overrightarrow{l_1}$ and $\overrightarrow{s_1}$, therefore lying on the C-plane, as does also $\overrightarrow{r_1}$. Distances $h_\pm$ from C-plane to either end of the tubular conductor.

$$\mathrm{d}B_1 = \frac{\mu_0}{4\pi\, r}\mathrm{d}I\left(\frac{h_+}{\sqrt{h_+^2 + r^2}} + \frac{h_-}{\sqrt{h_-^2 + r^2}}\right) \text{for } 0 \leqslant z_\mathrm{C} \leqslant L/2, \tag{2}$$

where $r = |\overrightarrow{r_1}|$, the distances $h_\pm$ are defined in figure 1 and related to z_C as

$$h_\pm = \sqrt{\left(\frac{L}{2} \pm z_\mathrm{C}\right)^2}, \tag{3}$$

the distance from P to either end of the wire segment being $\sqrt{h_\pm^2 + r^2}$. Moreover, see figure 2, for any segment 1 that contributes $\mathrm{d}\overrightarrow{B_1}$ to the magnetic field at P, there is a segment 2 at the same distance r from P and whose contribution $\mathrm{d}\overrightarrow{B_2}$ to the magnetic field has the same magnitude as $\mathrm{d}\overrightarrow{B_1}$, so that the added contribution of both segments to the magnetic field at P, i.e. $\mathrm{d}\overrightarrow{B_1} + \mathrm{d}\overrightarrow{B_2}$, is tangential to C, giving a net contribution $\mathrm{d}\overrightarrow{B}$ of *each* segment to the magnetic field of (see figure 2)

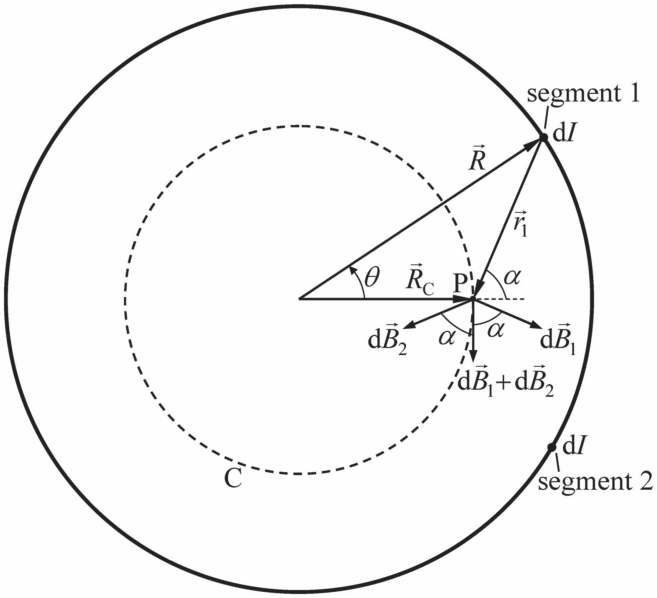

Figure 2. Cross-sectional view of tubular conductor in figure 1, showing two segments (1 and 2) equidistant from P and traversed by elementary currents dI (directed out of page), whose contributions to the field at P, $d\overrightarrow{B_1}$ and $d\overrightarrow{B_2}$, result in the combined contribution $d\overrightarrow{B_1} + d\overrightarrow{B_2}$ tangential to curve C. The angle between position vectors $\overrightarrow{R}$ and $\overrightarrow{R_C}$ is θ, and that between position vectors $\overrightarrow{R_C}$ and $(-\overrightarrow{r_1})$ is α. Note that cos α can be positive or negative depending on θ.

$$d\overrightarrow{B} = -\hat{\theta}\, dB_1 \cos\alpha, \tag{4}$$

where dB_1 is given by (2), α is the angle between $\overrightarrow{R_C}$ and $(-\overrightarrow{r_1})$ in figure 2, and $\hat{\theta}$ the unit vector tangential to C at P and oriented in the rotation direction of a right-handed corkscrew which is placed on the z-axis and advances with current I. The infinitesimal current dI through each segment is, see figure 1

$$dI = \frac{I}{2\pi R} R d\theta = \frac{I}{2\pi} d\theta \tag{5}$$

so that from (2)

$$dB_1 = \frac{\mu_0 I}{8\pi^2 r}\left(\frac{h_+}{\sqrt{h_+^2 + r^2}} + \frac{h_-}{\sqrt{h_-^2 + r^2}}\right) d\theta \tag{6}$$

and, inserting the latter into (4), the elementary segment's magnetic field $d\overrightarrow{B}$ is written as

$$d\overrightarrow{B} = -\hat{\theta}\frac{\mu_0 I}{8\pi^2 r}\left(\frac{h_+}{\sqrt{h_+^2 + r^2}} + \frac{h_-}{\sqrt{h_-^2 + r^2}}\right)\cos\alpha d\theta. \tag{7}$$

The magnetic field generated at P results from integrating (7), which requires that all quantities be expressed as functions of the same integration variable. From figure 2, r and cos α can be written as functions of θ as

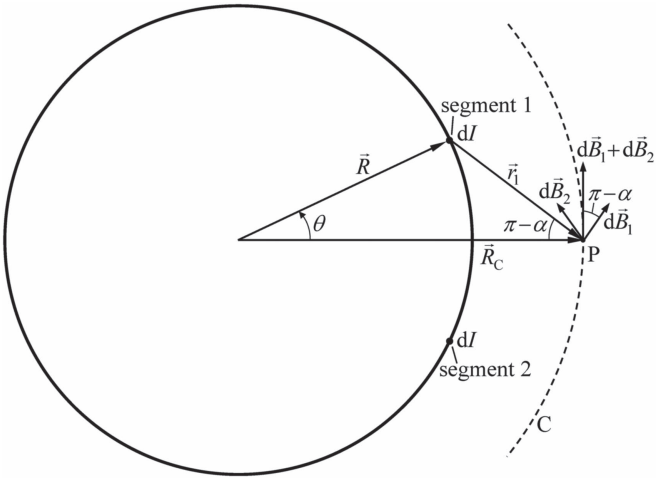

Figure 3. Identical setup to figure 2, save that point P is now located *outside* the tubular conductor, i.e. $R_C > R$. Segment currents dI directed out of page. From Biot–Savart's law the contributions of segments 1 and 2 to the field at P ($d\vec{B}_1$ and $d\vec{B}_2$) have the directions shown, so that the added contribution $d\vec{B}_1 + d\vec{B}_2$, although again tangential to C, now has the opposite orientation to that resulting from the two segments shown in figure 2. By contrast to figure 2, the values of $\cos\alpha = -\cos(\pi - \alpha)$ are now always negative, regardless of θ.

$$\cos\alpha = \frac{R\cos\theta - R_C}{r}, \tag{8a}$$

$$r = \sqrt{R_C^2 + R^2 - 2RR_C\cos\theta} \tag{8b}$$

so that (7) can be integrated as

$$\begin{aligned}\vec{B} &= -\hat{\theta}\frac{\mu_0 I}{8\pi^2}\int_0^{2\pi}\left(\frac{h_+}{\sqrt{h_+^2+r^2}} + \frac{h_-}{\sqrt{h_-^2+r^2}}\right)\frac{\cos\alpha}{r}\mathrm{d}\theta \\ &= -\hat{\theta}\frac{\mu_0 I}{4\pi^2}\int_0^{\pi}\left(\frac{h_+}{\sqrt{h_+^2+r^2}} + \frac{h_-}{\sqrt{h_-^2+r^2}}\right)\frac{\cos\alpha}{r}\mathrm{d}\theta \text{ for } 0 \leqslant z_C \leqslant L/2,\end{aligned} \tag{9}$$

the last step in (9) resulting from the already addressed equality between the contributions to the magnetic field at P from any pair of segments 1 and 2 in figure 2. Naturally, as the flow of current in the finite length tubular conductor requires such conductor to be integrated in some circuit, e.g. [10], equation (9) has to be understood as the finite tube's contribution to the circuit's magnetic field. Moreover, although (9) was derived using figures 1 and 2, which correspond to $R_C < R$, it is also valid for $R_C > R$, the case shown in figure 3, because (1)–(8) are mathematically identical in both cases. However, from a physical perspective, there are significant differences between the two, as next highlighted.

2.2. Magnetic field inside ($R_C < R$) and outside ($R_C > R$) of the finite tube

Although (9) does not explicitly differentiate between $R_C < R$ and $R_C > R$, there is an implicit distinction which follows from Biot–Savart's law (1), and thus from (2) to (8), and

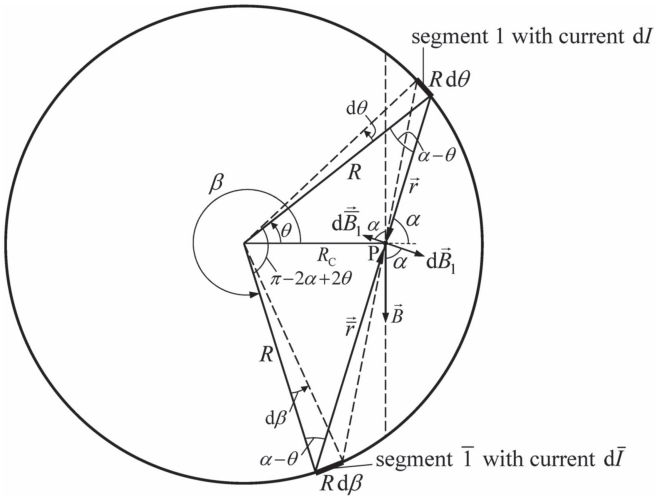

Figure 4. Shows opposing contributions to the field at P, $\mathrm{d}\overrightarrow{B_1}$ and $\mathrm{d}\overrightarrow{\bar{B}_1}$, generated respectively by oppositely-located segments 1 and $\bar{1}$, of widths $R\mathrm{d}\theta$ and $R\mathrm{d}\beta$, traversed by elementary currents $\mathrm{d}I$ and $\mathrm{d}\bar{I}$ directed out of the page. While segment $\bar{1}$ is further from P than segment 1 it does transport more current due to its larger width, so that from (5), (12), (16), (17) $\mathrm{d}\bar{I}/\bar{r} = \mathrm{d}I/r$ and thus, see (11) with (2), the strength of $\mathrm{d}\overrightarrow{\bar{B}_1}$ relative to $\mathrm{d}\overrightarrow{B_1}$ depends *solely* on r, $\bar{r}$, and $h_\pm$.

can be interpreted as follows: for $R_\mathrm{C} > R$, see figure 3 with (8*a*), $\cos\alpha$ is always negative and thus all contributions (4) to $\overrightarrow{B}$ point in the same direction $(+\hat{\theta})$, i.e. for $R_\mathrm{C} > R$ the field $\overrightarrow{B}$ is oriented in the rotation direction of an axially-placed right-handed corkscrew that advances with current I, in line with [12]. By contrast, for $R_\mathrm{C} < R$, see figure 2 with (8*a*), $\cos\alpha$ is positive for $0 \leqslant \theta < \cos^{-1}(R_\mathrm{C}/R)$ and $2\pi - \cos^{-1}(R_\mathrm{C}/R) < \theta \leqslant 2\pi$ and negative for $\cos^{-1}(R_\mathrm{C}/R) < \theta < 2\pi - \cos^{-1}(R_\mathrm{C}/R)$, and thus contributions (4) to $\overrightarrow{B}$ point in the $(-\hat{\theta})$ direction in the former intervals and in the $(+\hat{\theta})$ direction in the latter one. The combined effect of such opposing contributions, only present for $R_\mathrm{C} < R$, is best understood by recasting (9) for this case using figure 4.

From figure 4, for any segment 1 of width $R\mathrm{d}\theta$ that provides a net contribution to the field at P of $-\hat{\theta}\mathrm{d}B_1\cos\alpha$, there is an oppositely-located segment $\bar{1}$ of width $R\mathrm{d}\beta$ that provides an opposing net contribution $\hat{\theta}\mathrm{d}\bar{B}_1\cos\alpha$, where $\mathrm{d}\overrightarrow{\bar{B}_1}$ is the field generated at P by segment $\bar{1}$, the combined net contributions of 1 and $\bar{1}$ being thus

$$\mathrm{d}\overrightarrow{B} = -\hat{\theta}(\mathrm{d}B_1 - \mathrm{d}\bar{B}_1)\cos\alpha. \tag{10}$$

To determine (10) first note that, by analogy with (2),

$$\mathrm{d}\bar{B}_1 = \frac{\mu_0}{4\pi\,\bar{r}}\mathrm{d}\bar{I}\left(\frac{h_+}{\sqrt{h_+^2+\bar{r}^2}} + \frac{h_-}{\sqrt{h_-^2+\bar{r}^2}}\right), \tag{11}$$

where, in figure 4, $\bar{r}$ is the distance from P to segment $\bar{1}$, and $\mathrm{d}\bar{I}$ the infinitesimal current through such segment, which by analogy with (5) is

$$\mathrm{d}\bar{I} = \frac{I}{2\pi}\mathrm{d}\beta, \tag{12}$$

thereby reducing the problem of determining (10) to that of determining infinitesimal angle $\mathrm{d}\beta$ and distance $\bar{r}$ in figure 4. In figure 4 the triangle of side $r + \bar{r}$ is isosceles, its other 2 sides (of length R) forming an angle of $\pi - 2\alpha + 2\theta$, so that $\beta = \pi + 2\alpha - \theta$ and thus

$$\mathrm{d}\beta = 2\mathrm{d}\alpha - \mathrm{d}\theta. \tag{13}$$

Also, from (8)

$$\alpha = \cos^{-1}\left(\frac{R\cos\theta - R_\mathrm{C}}{\sqrt{R_\mathrm{C}^2 + R^2 - 2RR_\mathrm{C}\cos\theta}}\right), \tag{14}$$

and therefore

$$\mathrm{d}\alpha = \frac{R - R_\mathrm{C}\cos\theta}{R_\mathrm{C}^2 + R^2 - 2RR_\mathrm{C}\cos\theta}R\mathrm{d}\theta. \tag{15}$$

Inserting (15) into (13) and using (8*b*) gives

$$\mathrm{d}\beta = \frac{R^2 - R_\mathrm{C}^2}{r^2}\mathrm{d}\theta. \tag{16}$$

On the other hand, from figure 4 and elementary geometry,

$$\bar{r} = \frac{R^2 - R_\mathrm{C}^2}{r} \tag{17}$$

so that, using (12), (16) and (17), (11) can be written as

$$\mathrm{d}\bar{B}_\mathrm{I} = \frac{\mu_0 I}{8\pi^2 r}\left(\frac{h_+}{\sqrt{h_+^2 + \bar{r}^2}} + \frac{h_-}{\sqrt{h_-^2 + \bar{r}^2}}\right)\mathrm{d}\theta. \tag{18}$$

Inserting (6) and (18) into (10), the combined contributions to $\mathrm{d}\vec{B}$ of any pair of segments 1 and $\bar{1}$ in figure 4 can be rearranged as

$$\mathrm{d}\vec{B} = -\hat{\theta}\frac{\mu_0 I}{8\pi^2 r}\left[\left(\frac{h_+}{\sqrt{h_+^2 + r^2}} - \frac{h_+}{\sqrt{h_+^2 + \bar{r}^2}}\right) + \left(\frac{h_-}{\sqrt{h_-^2 + r^2}} - \frac{h_-}{\sqrt{h_-^2 + \bar{r}^2}}\right)\right]\cos\alpha\mathrm{d}\theta. \tag{19}$$

If the contributions (19) to $\mathrm{d}\vec{B}$ generated by each pair of segments 1 and $\bar{1}$ in figure 4 are added from $\alpha = 0$ (i.e. $\theta = 0$) to $\alpha = \pi/2$ (i.e. $\theta = \cos^{-1}(R_\mathrm{C}/R)$), thereby spanning half the tubular conductor, from symmetry the remaining half will yield an identical contribution to the field because, as discussed earlier in the context of figure 2, for any segment 1 (or $\bar{1}$) there is always a paired segment 2 (or $\bar{2}$) equidistant from P. Therefore, from (19), for the case

$R_C < R$, (9) can be recast as

$$\overrightarrow{B} = -\hat{\theta}\frac{\mu_0 I}{4\pi^2}\int_0^{\cos^{-1}(R_C/R)}\left[\left(\frac{h_+}{\sqrt{h_+^2 + r^2}} - \frac{h_+}{\sqrt{h_+^2 + \bar{r}^2}}\right) + \left(\frac{h_-}{\sqrt{h_-^2 + r^2}} - \frac{h_-}{\sqrt{h_-^2 + \bar{r}^2}}\right)\right]\frac{\cos\alpha}{r}\mathrm{d}\theta \text{ for } 0 \leqslant z_C \leqslant L/2 \text{ with } R_C < R \tag{20}$$

with r, $\bar{r}$ and $\cos\alpha$ being given by (8) with (17) as functions of integration variable θ. Carefully note that in the integration interval of (20), α goes from 0 to $\pi/2$ and thus $\cos\alpha$ is always positive. Moreover, since in such interval $r < \bar{r}$ (figure 4), both curve-bracketed terms in (20) are positive. Therefore the integrating function (20) is always positive, so that for any point P located at $R_C < R$ the field $\overrightarrow{B}$ has the direction $(-\hat{\theta})$, i.e. counter to the rotation direction of an axially-placed right-handed corkscrew that advances with the current I, again in line with [12]. Moreover, from (3), an increase in L and therefore in $h_\pm$ results in a decrease in value of the curve-bracketed terms in (19) and (20) and thus of the individual contributions $\mathrm{d}\overrightarrow{B}$ for $R_C < R$, i.e. an increase in tubular conductor length weakens the magnetic field within it, ultimately leading to $\overrightarrow{B} = \overrightarrow{0}$. Conversely, for $R_C > R$, an increase in L and therefore $h_\pm$ results in an increase in value of the curve-bracketed terms in (7) and (9) and thus of the individual contributions $\mathrm{d}\overrightarrow{B}$ for $R_C > R$. Therefore, and since $\cos\alpha$ never changes sign in the integration interval of (9) for $R_C > R$ (see (8*a*) with figure 3), all $\mathrm{d}\overrightarrow{B}$ contributions are additive and an increase in tube length strengthens the magnetic field.

2.3. Extension to $z_C > L/2$

Given that the process used to determine the magnetic field for $z_C > L/2$ parallels that for $0 \leqslant z_C \leqslant L/2$ a detailed analysis is redundant, the basic difference being that for $z_C > L/2$ independent variable h_- needs to be replaced by $(-h_-)$ in all relevant expressions. Applying such operation to (9), the magnetic field for both $R_C > R$ and $R_C < R$ is given by

$$\begin{aligned}\overrightarrow{B} &= -\hat{\theta}\frac{\mu_0 I}{4\pi^2}\int_0^{\pi}\left(\frac{h_+}{\sqrt{h_+^2 + r^2}} - \frac{h_-}{\sqrt{h_-^2 + r^2}}\right)\frac{\cos\alpha}{r}\mathrm{d}\theta \\ &= -\hat{\theta}\frac{\mu_0 I}{4\pi^2}\int_0^{\pi}\left(\frac{1}{\sqrt{1 + (r/h_+)^2}} - \frac{1}{\sqrt{1 + (r/h_-)^2}}\right)\frac{\cos\alpha}{r}\mathrm{d}\theta \text{ for } z_C > L/2,\end{aligned} \tag{21}$$

where, since $h_+ > h_-$, the curve-bracketed term is *always* positive. For $R_C > R$, the term $\cos\alpha$ in (21) is negative (figure 3), which combined with the positive curve-bracketed term in (21) gives a negatively-valued integrating function and thus $\overrightarrow{B}$ is oriented in the $(+\hat{\theta})$ direction, i.e. for $R_C > R$ the direction of $\overrightarrow{B}$ in the region $z_C > L/2$ is the same as that in $0 \leqslant z_C \leqslant L/2$. By contrast this is not necessarily the case for $R_C < R$, as next explained. For $z_C > L/2$, since h_- needs to be replaced by $(-h_-)$, (20) has to be modified to

$$\overrightarrow{B} = -\hat{\theta}\frac{\mu_0 I}{4\pi^2}\int_0^{\cos^{-1}(R_C/R)}\left[\left(\frac{h_+}{\sqrt{h_+^2+r^2}}-\frac{h_+}{\sqrt{h_+^2+\bar{r}^2}}\right)\right.$$
$$\left.-\left(\frac{h_-}{\sqrt{h_-^2+r^2}}-\frac{h_-}{\sqrt{h_-^2+\bar{r}^2}}\right)\right]\frac{\cos\alpha}{r}\mathrm{d}\theta \text{ for } z_C > L/2 \text{ with } R_C < R \qquad (22)$$

i.e. although $\cos\alpha$ in (22) is positive (figure 2), and both curve-bracketed terms in (22) remain identical to the corresponding ones in (20) and thus positive-valued, instead of adding they now subtract. Since such difference is not necessarily positive, the magnetic field direction for $R_C < R$ is no longer necessarily $(-\hat{\theta})$, a result whose interpretation was lacking in [12] and is best illustrated by two examples, namely the magnetic field close to the basal plane $z_C = L/2$ (so that, from (3), $h_- \approx 0$), and distant from such plane ($z_C \gg L/2$, i.e. large $h_\pm$). In the first example ($h_- \approx 0$), the second curve-bracketed term in (22) is negligible and therefore the integrating function in (22) is always positive, i.e. $\overrightarrow{B}$ is oriented in the $(-\hat{\theta})$ direction. By contrast, in the second example (large $h_\pm$) the square-bracketed term in (22) approximates as $\frac{1}{2}\left(\frac{1}{h_+^2}-\frac{1}{h_-^2}\right)(\bar{r}^2-r^2) < 0$ giving a negative integrating function in (22), i.e. $\overrightarrow{B}$ is oriented in the $(+\hat{\theta})$ direction. It is instructive, from a physical perspective, to visualise such behaviour through figure 4: as $h_\pm$ increases, the magnitude of each $\mathrm{d}\overrightarrow{B_1}$ contribution in figure 4 becomes *smaller* than that of the opposing contribution $\mathrm{d}\overrightarrow{B_1}$, the net result being that the field $\overrightarrow{B}$ in this figure reverses direction. This counterintuitive result, which shows that the fields for $R_C < R$ and $R_C > R$ can both point in the same direction, physically differentiates this region from $0 \leqslant z_C \leqslant L/2$.

2.4. Numerical comparison to earlier work

At the outset it is important to clarify that unlike the present study, the magnetic field equations in [12] were not derived from the Biot–Savart law and were not identical to (9) or (21), but were instead derived using an oblique solid angle formula in the magnetic field circulation expression obtained in [14] from the application of Ampère–Maxwell's law to an arbitrarily-shaped finite length wire in the zero retarded-time limit, resulting in [12]

$$\overrightarrow{B} = \hat{\theta}\frac{\mu_o I}{4\pi^2}\frac{\pi}{R_C}(\sigma_+ + \sigma_- - 2) \quad \text{for } 0 \leqslant z_C \leqslant L/2 \text{ with } R_C < R, \qquad (23a)$$

$$\overrightarrow{B} = \hat{\theta}\frac{\mu_o I}{4\pi^2}\frac{\pi}{R_C}(\sigma_+ + \sigma_-) \quad \text{for } 0 \leqslant z_C \leqslant L/2 \text{ with } R_C > R, \qquad (23b)$$

$$\overrightarrow{B} = \hat{\theta}\frac{\mu_o I}{4\pi^2}\frac{\pi}{R_C}(\sigma_+ - \sigma_-) \quad \text{for } z_C > L/2, \qquad (23c)$$

where

$$\sigma_\pm = \frac{1}{\pi}\int_0^\pi \frac{h_\pm \mathrm{d}\gamma}{\sqrt{h_\pm^2 + R^2 + R_C^2 + 2RR_C\cos\gamma}}\frac{h_\pm^2 + R^2 + RR_C\cos\gamma}{h_\pm^2 + R^2\sin^2\gamma}. \qquad (24)$$

Despite (9) and (21) being different from (23) with (24), limited comparison between both sets of equations gave identical numerical results, shown in figures 5 and 6, such identity being consistent with both Biot–Savart's law and the equations derived in [12] being valid in the zero retarded-time limit, as well as with the very recent result that the circulation

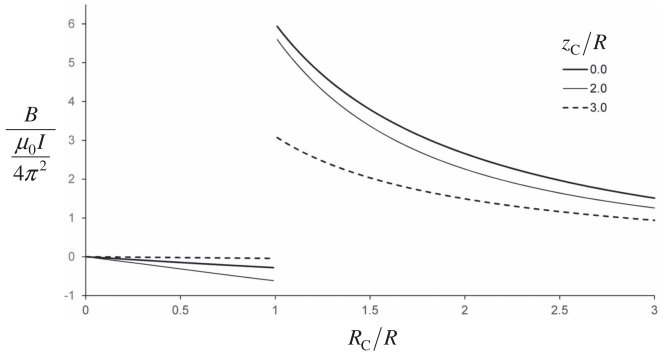

Figure 5. Magnetic field (normalised to $\mu_0 I_0/4\pi^2$) versus R_C/R, at different normalised positions (z_C/R) for $0 \leqslant z_C \leqslant L/2$. Field values obtained from equation (9) with (8) and (3) coincide numerically with those obtained from equations (23*a*), (23*b*) with (24) and (3). Here $L = 6R$, so that curves $z_C/R = 0.0,\ 2.0,\ 3.0$ correspond respectively to $z_C = 0.0,\ 0.67L/2,\ L/2$.

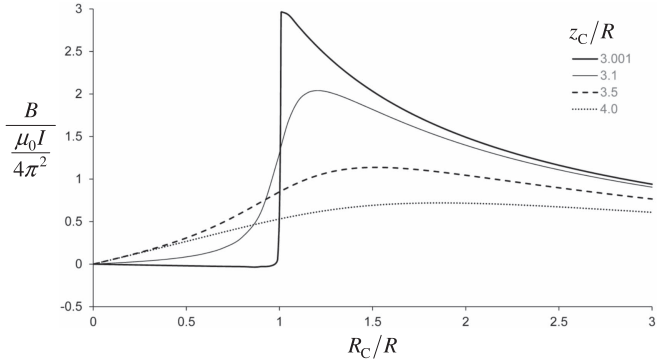

Figure 6. Magnetic field (normalised to $\mu_0 I_0/4\pi^2$) versus R_C/R, at different normalised positions (z_C/R) for $z_C > L/2$. Field values obtained from equation (21) with (8) and (3) coincide numerically with those obtained from equation (23*c*) with (24) and (3). Here $L = 6R$, so that curves $z_C/R = 3.001,\ 3.1,\ 3.5,\ 4.0$ correspond respectively to $z_C = 1.0003L/2,\ 1.03L/2,\ 1.17L/2,\ 1.33L/2$.

expression derived in [14] and used in [12] is, in fact, the magnetic field circulation counterpart to Biot–Savart's law for a volume distribution of current in the filamentary wire limit [27]. Additionally such identity corroborates, indirectly, the oblique solid angle formula which was derived and used in [12].

2.5. Simplified expressions for the magnetic field

2.5.1. The finite tube axis vicinity ($R_C \ll R$). The magnetic field can be simplified in the tube axis vicinity by first inserting (8*b*) into the $1\Big/\sqrt{h_\pm^2 + r^2}$ terms of (9) and (21), which can then be approximated as

$$\frac{1}{\sqrt{h_\pm^2+r^2}}=\frac{1}{\sqrt{h_\pm^2+R^2}}\left(1+\frac{R_C^2-2RR_C\cos\theta}{h_\pm^2+R^2}\right)^{-1/2}$$
$$\approx\frac{1}{\sqrt{h_\pm^2+R^2}}\left(1-\frac{1}{2}\frac{R_C^2}{h_\pm^2+R^2}+\frac{RR_C}{h_\pm^2+R^2}\cos\theta\right) \tag{25}$$

provided the inequality

$$R_C\ll\sqrt{h_\pm^2+R^2} \tag{26}$$

holds, which is always the case in the tube axis vicinity. From (8) with (25), the terms in (9) and (21) can be written and rearranged in the form

$$\frac{1}{\sqrt{h_\pm^2+r^2}}\frac{\cos\alpha}{r}\approx\frac{1}{\sqrt{h_\pm^2+R^2}}\left(1-\frac{1}{2}\frac{R_C^2}{h_\pm^2+R^2}+\frac{RR_C}{h_\pm^2+R^2}\cos\theta\right)$$
$$\times\frac{R\cos\theta-R_C}{R_C^2+R^2-2RR_C\cos\theta}=-\frac{1}{2R_C}\frac{1}{\sqrt{h_\pm^2+R^2}}$$
$$\times\left[1+\frac{1}{2}\frac{R^2-2R_C^2}{h_\pm^2+R^2}+\left(1+\frac{1}{2}\frac{R^2}{h_\pm^2+R^2}\right)\right.$$
$$\left.\times\frac{R_C^2-R^2}{R_C^2+R^2-2RR_C\cos\theta}+\frac{RR_C}{h_\pm^2+R^2}\cos\theta\right] \tag{27}$$

so they then integrate as

$$\int_0^\pi\frac{1}{\sqrt{h_\pm^2+r^2}}\frac{\cos\alpha}{r}\mathrm{d}\theta\approx-\frac{1}{2R_C}\frac{1}{\sqrt{h_\pm^2+R^2}}\left\{\left[1+\frac{1}{2}\frac{R^2-2R_C^2}{h_\pm^2+R^2}\right]\pi\right.$$
$$+\left(1+\frac{1}{2}\frac{R^2}{h_\pm^2+R^2}\right)(R_C^2-R^2)\frac{2}{R_C+R}\frac{1}{|R_C-R|}\left.\left[\tan^{-1}\left(\frac{R_C+R}{|R_C-R|}\tan\frac{\theta}{2}\right)\right]_{\theta=0}^{\theta=\pi}\right\}$$
$$=-\frac{1}{R_C}\frac{1}{\sqrt{h_\pm^2+R^2}}\left[1+\frac{1}{2}\frac{R^2-2R_C^2}{h_\pm^2+R^2}+\left(1+\frac{1}{2}\frac{R^2}{h_\pm^2+R^2}\right)\frac{R_C-R}{|R_C-R|}\right]\frac{\pi}{2}. \tag{28}$$

Given that only the case $R_C<R$ is of interest here, the above integral gives $R_C(h_\pm^2+R^2)^{-3/2}\pi/2$, which inserted into (9) and (21) results in two expressions that approximate the magnetic field in the tube axis vicinity as

$$\vec{B}\approx-\hat{\theta}\frac{\mu_0 I}{4\pi^2}\left[\frac{h_+}{(h_+^2+R^2)^{3/2}}+\frac{h_-}{(h_-^2+R^2)^{3/2}}\right]\frac{\pi}{2}R_C\ \text{ for }\ 0\leqslant z_C\leqslant L/2\ \text{ with }\ R_C\ll R, \tag{29a}$$

$$\vec{B}\approx-\hat{\theta}\frac{\mu_0 I}{4\pi^2}\left[\frac{h_+}{(h_+^2+R^2)^{3/2}}-\frac{h_-}{(h_-^2+R^2)^{3/2}}\right]\frac{\pi}{2}R_C\ \text{ for }\ z_C>L/2\ \text{ with }\ R_C\ll R. \tag{29b}$$

Comparing (29) to the numerical results given earlier shows that the linear dependence of B on R_C, present in (29), is observed in figures 5 and 6 up to about $R_C = 0.2R$ and, for some of the curves, well beyond that, an observation which can be interpreted by noting that away from the axis vicinity (i.e. for larger R_C), condition (26) will remain valid provided that $h_\pm$ is also large. However, being conservative, the deviation of (29) relative to the general solution curves in figures 5 and 6 is under 2% at $R_C = 0.1R$, rising to under 8% at $R_C = 0.2R$.

2.5.2. Region near the median plane just outside the finite tube. This approximation is only possible if the tube length is large in comparison to its radius, i.e. if $L \gg R$. For such case near the median plane $h_\pm \gg R$, which combined with the condition of being just outside the tube gives $R_C^2 \ll h_\pm^2$ and $RR_C \ll h_\pm^2 + R^2$, so that equations (25)–(28) remain valid and, since in this case $R_C > R$, equation (28) gives

$$\int_0^\pi \frac{1}{\sqrt{h_\pm^2 + r^2}} \frac{\cos\alpha}{r} \mathrm{d}\theta \approx \frac{1}{(h_\pm^2 + R^2)^{3/2}} \frac{\pi}{2} \frac{R_C^2 - R^2}{R_C} - \frac{1}{\sqrt{h_\pm^2 + R^2}} \frac{\pi}{R_C}. \tag{30}$$

Inserting (30) into (9) gives the approximate closed form expression for the magnetic field near the median plane just outside the tube as

$$\begin{aligned} \overrightarrow{B} \approx \hat{\theta} \frac{\mu_0 I}{4\pi^2} \Bigg\{ \Bigg\{ \left[\frac{h_+}{(h_+^2 + R^2)^{3/2}} + \frac{h_-}{(h_-^2 + R^2)^{3/2}} \right] R^2 + 2 \left(\frac{h_+}{\sqrt{h_+^2 + R^2}} + \frac{h_-}{\sqrt{h_-^2 + R^2}} \right) \Bigg\} \\ \times \frac{\pi}{2} \frac{1}{R_C} - \left[\frac{h_+}{(h_+^2 + R^2)^{3/2}} + \frac{h_-}{(h_-^2 + R^2)^{3/2}} \right] \frac{\pi}{2} R_C \Bigg\}, \end{aligned} \tag{31}$$

i.e. the magnetic field is of the form $C_1/R_C + C_2 R_C$, constants C_1 and C_2 depending both on the finite tube geometry and on the position of the point of interest relative to the two basal planes. Naturally, if the tube is infinitely long ($L \to \infty$), from (3) $h_\pm \to \infty$ and (31) reduces to the well-known result $B_\theta = \mu_0 I/(2\pi R_C)$.

2.5.3. Region very far outside the finite tube. This last approximation corresponds to the trivial case where application of condition $R_C \gg R$ to (8) results in $\cos\alpha \approx -R_C/R$ and $r \approx R_C$, so that (9) and (21) reduce to the approximate closed form expressions

$$\overrightarrow{B} \approx \hat{\theta} \frac{\mu_0 I}{4\pi R_C} \left[\frac{h_+}{\sqrt{h_+^2 + R^2}} + \frac{h_-}{\sqrt{h_-^2 + R^2}} \right] \text{ for } 0 \leqslant z_C \leqslant L/2 \text{ with } R_C \gg R, \tag{32a}$$

$$\overrightarrow{B} \approx \hat{\theta} \frac{\mu_0 I}{4\pi R_C} \left[\frac{h_+}{\sqrt{h_+^2 + R^2}} - \frac{h_-}{\sqrt{h_-^2 + R^2}} \right] \text{ for } z_C > L/2 \text{ with } R_C \gg R, \tag{32b}$$

i.e. as would be expected the tubular conductor's magnetic field becomes indistinguishable from that generated by a filamentary wire segment of identical length.

2.6. The finite length solenoid magnetic field's azimuthal component

In addition to the widely studied axial and radial components, e.g. [8, 28–39], the magnetic field generated by a tightly wound solenoid has a weaker azimuthal component which can be readily

evaluated, an analysis which has hitherto been restricted to the infinitely long solenoid [16–25]. While readily conceding Gauthier's [21] point that the following does not apply to solenoids with an even number of superimposed windings, the magnetic field generated by a tightly wound odd-layered solenoid of finite length includes a term resulting from the component of the current flowing along the solenoid's surface, such term being precisely the magnetic field generated by the finite tubular conductor described in the present study and in [12]. Therefore, while an infinitely long solenoid of radius R generates a weak azimuthal magnetic field in the region surrounding it [16–25], for a finite length solenoid our results showed that such azimuthal component is present not only in the region surrounding the solenoid, $R_C > R$, but also in the region inside it, $R_C < R$, such component simplifying to (29) in the solenoid axis vicinity, to (31) near the median plane just outside the solenoid, and to (32) very far outside the solenoid (i.e. $R_C \gg R$). Moreover, increased solenoid length results in the strengthening of such azimuthal component outside the solenoid and weakening within it, ultimately leading to the well-known limiting values $B_\theta = \mu_0 I/(2\pi R_C)$ and $B_\theta = 0$ respectively.

3. Conclusions

General solutions for the magnetic field generated by a conducting tube of length L and radius R carrying a current in the axial direction were obtained from Biot–Savart's law and symmetry considerations for points P of z-coordinates $0 \leqslant z_C \leqslant L/2$ relative to the tube's mid-plane and located at distances $0 \leqslant R_C < \infty$ from its axis. Inside the tube ($R_C < R$) the magnetic field orientation, which was counter to the rotation direction of a right-handed corkscrew placed on its axis and advancing with the current, was interpreted from Biot–Savart's law as resulting from opposing contributions that originated from diametrically-opposite ends of the tube relative to P. It was also found that no such competing effects were present for points located outside the tube ($R_C > R$), that the magnetic field outside the tube had reverse orientation to that inside it, and that an increase in tube length led to weakening of the magnetic field inside it and strengthening of such field outside it. The region $z_C > L/2$ was also addressed and it was shown that, contrary to the region $0 \leqslant z_C \leqslant L/2$, the magnetic field's orientation for $R_C < R$ was not necessarily opposite to that for $R_C > R$. Additionally, simplified approximate closed form expressions for the magnetic field were derived in the tube axis vicinity, near the median plane just outside the tube, and very far outside the tube (i.e. $R_C \gg R$). Finally, the azimuthal component of the finite solenoid magnetic field was addressed using the finite tube results which showed that, by contrast to the infinite solenoid, such component was present not only outside ($R_C > R$) the solenoid but also within it, an increase in solenoid length resulting in the strengthening of such component outside the solenoid and weakening within it.

ORCID iDs

Joaquim Anacleto https://orcid.org/0000-0002-0299-0146

References

[1] Macklin P A 1973 Ampere, Biot–Savart and straight wire *Bull. Am. Phys. Soc.* **18** 890–1
[2] Kalhor H A 1988 Comparison of Ampere's circuital law (ACL) and the law of Biot–Savart (LBS) *IEEE Trans. Educ.* **31** 236–8
[3] Kalhor H A 1990 The degree of intelligence of the law of Biot–Savart *IEEE Trans. Educ.* **33** 365–6

[4] Charitat T and Graner F 2003 About the magnetic field of a finite wire *Eur. J. Phys.* **24** 267–70
[5] Fishbane P M, Gasiorowicz S G and Thornton S G 2005 *Physics for Scientists and Engineers with Modern Physics* 3rd edn (London/Englewood Cliffs, NJ: Pearson/Prentice-Hall)
[6] Jiménez J L, Campos I and Aquino N 2008 Exact electromagnetic fields produced by a finite wire with constant current *Eur. J. Phys.* **29** 163–75
[7] Hayt W H and Buck J A 2012 *Engineering Electromagnetics* 8th edn (New York: McGraw-Hill)
[8] Griffiths D J 2014 *Introduction to Electrodynamics* 4th edn (Harlow: Pearson Education)
[9] Barchiesi D 2014 Didactical formulation of the Ampère law *Eur. J. Phys.* **35** 038001
[10] Morvay B and Pálfalvi L 2015 On the applicability of Ampère's law *Eur. J. Phys.* **36** 065014
[11] Ferreira J M and Anacleto J 2015 Comment on exact electromagnetic fields produced by a finite wire with constant current *Eur. J. Phys.* **37** 048002
[12] Ferreira J M and Anacleto J 2017 Magnetic field created by a conducting cylindrical shell of finite length *Electr. Eng.* **99** 979–86
[13] Ferreira J M and Anacleto J 2018 Magnetic field generated by the flow of AC current through finite length nonmagnetic conductors (cylinders, tubes, coaxial cables) *Electr. Eng.* in press (https://doi.org/10.1007/s00202-017-0588-1)
[14] Ferreira J M and Anacleto J 2013 Ampère–Maxwell law for a conducting wire: a topological perspective *Eur. J. Phys.* **34** 1403–10
[15] Halliday D, Resnick R and Walker J 2012 *Principles of Physics* 9th edn (New Delhi: Wiley India)
[16] Ford W 1972 *Classical and Modern Physics* vol 2 (Lexington, KY: Xerox College)
[17] Williams D H and Sprangler J 1981 *Physics for Science and Engineering* (New York: Van Nostrand-Reinhold)
[18] Sandin T R 1984 Don't forget the pitch *Am. J. Phys.* **52** 679
[19] Harada M 1986 On the magnetic field of a solenoid *Am. J. Phys.* **54** 1065
[20] Wangsness R K 1986 *Electromagnetic Fields* 2nd edn (New York: Wiley)
[21] Gauthier N 1987 Solenoids and the Aharonov–Bohm effect *Am. J. Phys.* **55** 393
[22] Lorraine P and Corson D R 1990 *Electromagnetism: Principles and Applications* 2nd edn (San Francisco, CA: Freeman)
[23] Tominaka T 2006 Magnetic field calculation of an infinitely long solenoid *Eur. J. Phys.* **27** 1399–408
[24] Serway R A and Jewett J W Jr 2013 *Physics for Scientists and Engineers with Modern Physics* 9th edn (Boston, MA: Cengage Learning)
[25] Pathak A 2017 An elementary argument for the magnetic field outside a solenoid *Eur. J. Phys.* **38** 015201
[26] Griffiths D J and Heald M A 1991 Time-dependent generalizations of the Biot–Savart and Coulomb laws *Am. J. Phys.* **59** 111–7
[27] Ferreira J M and Anacleto J 2018 The magnetic field circulation counterpart to Biot–Savart's law *Eur. Phys. J. Plus* **133** 234
[28] Barker J R 1949 The magnetic field inside a solenoid *Br. J. Appl. Phys.* **1** 65–7
[29] Callaghan E E and Maslen S H 1960 The magnetic field of a finite solenoid *NASA Technical Note* D-465 (http://ntrs.nasa.gov/archive/nasa/casi.ntrs.nasa.gov/19980227402.pdf)
[30] Dasgupta B 1984 Magnetic field due to a solenoid *Am. J. Phys.* **53** 258
[31] Hauser W 1985 Note on 'Magnetic field due to a solenoid' *Am. J. Phys.* **53** 774
[32] Farley J and Price R H 2001 Field just outside a long solenoid *Am. J. Phys.* **69** 751–4
[33] Conway J T 2001 Exact solutions for the magnetic fields of axisymmetric solenoids and current distributions *IEEE Trans. Magn.* **37** 2977–88
[34] Chia C T and Wang Y F 2002 The magnetic field along the axis of a long finite solenoid *Phys. Teach.* **40** 288–9
[35] Espinosa O and Slusarenko V 2003 The magnetic field of an infinite solenoid *Am. J. Phys.* **71** 953–4
[36] Labinac V, Erceg N and Kotnik-Karuza D 2006 Magnetic field of a cylindrical coil *Am. J. Phys.* **74** 621–7
[37] Purcell E M and Morin D J 2013 Electricity and Magnetism 3rd edn (Cambridge: Cambridge University Press)
[38] Binder P, Hui K and Goldman J 2014 Magnetic fields at the center of coils *Phys. Teach.* **52** 560
[39] Liang M L and Wang T 2015 Calculating the magnetic field of the infinite solenoid and understanding the Ampere circuital law from the magnetic field of moving charges *Eur. J. Phys.* **36** 065043